Urban LULC Change Detection and Mapping Spatial Variations of Aurangabad City Using IRS LISS-III Temporal Datasets and Supervised Classification Approach

Ajay D. Nagne, Amol D. Vibhute, Rajesh K. Dhumal, Karbhari V. Kale and S. C. Mehrotra

Abstract An accurate mapping of urban LULC is essential for urban development and planning. Although urban area represents a little portion of Earth surface, which brings an unbalanced impact on its surrounding areas. However urban LULC mapping and change detection is critical issue by traditional methods. Recent advances in Geospatial technology can be used to map built-up areas for detecting the urban growth patterns. In this work IRS LISS-III sensors image data of 2003, 2009, and 2015 of same season were used. The LULC mapping and change detection was carried out by four supervised classifier namely Maximumlikelihood classifier (MLC), Mahalanobis-Distance (MD), Minimum-Distance-to-Means (MDM), and Parallelepiped classifier (PC). Obtained results were examined by considering the efficiency of each classifier to accurately map the identified LULC classes. It is observed that, MLC has given the highest overall accuracy of 73.07, 83.51, and 93.43% with kappa coefficient of 0.64, 0.78, and 0.90 in 2003, 2009, and 2015 respectively, which are superior among others; hence we have used classified layer obtained from MLC for further change detection and analysis from 2003 to 2015.

A. D. Nagne (✉) · A. D. Vibhute · R. K. Dhumal · K. V. Kale · S. C. Mehrotra
Department of CS & IT, Dr. Babasaheb Ambedkar Marathwada University, Aurangabad, Maharashtra, India
e-mail: ajay.nagne@gmail.com

A. D. Vibhute
e-mail: amolvibhute2011@gmail.com

R. K. Dhumal
e-mail: dhumal19@gmail.com

K. V. Kale
e-mail: kvkale91@gmail.com

S. C. Mehrotra
e-mail: mehrotra.suresh15j@gmail.com

P. Nagabhushan et al. (eds.), *Data Analytics and Learning*,
Lecture Notes in Networks and Systems 43,
https://doi.org/10.1007/978-981-13-2514-4_31

Keywords Urban classification · Spatial variation
Maximum likelihood classifier (MLC) · LULC · Change detection

1 Introduction

Land-Use (LU) and Land-Cover (LC) are two separate terminologies, which are often used interchangeably. The LC states the physical characteristics of earth's surface distribution, like rock, soil, water, vegetation, manmade structures and other features of the land. While LU indicates that, the land has been used by humans and their habitat. The LULC pattern is an outcome of natural and socioeconomic factors and their utilization by people [1]. To achieve the increasing demands for basic human needs and welfare; information on LULC and possibilities for their optimal use are essential for the formation and implementation of LU schemes [2].

An accurate temporal LULC change detection of Earth's surface objects are very significant to understand the interactions between humans and natural phenomena, in order to promote better decision-making. New strategies are required for the regular updating of existing databases rather than traditional methods. These are generally in view of field examinations and the visual understanding of Remote Sensing Images [3]. The usual techniques are tedious and costly, and mapping exercises frequently can't stay aware of the pace of urban improvement. Geospatial technology provides an extensive variety of applications which can be used for effective decision-making and future planning [4]. Application of geospatial technology made possible to study the LU pattern and identifies a changes in LC with better accuracy in less time. Under Geospatial approach, we have identified spatial variations of Aurangabad city from 2003 to 2015 using LISS-III data and supervised approach.

This paper is grouped into five sections. The introduction has been presented in Sect. 1. Section 2 illustrates the study area. Section 3 portrays the proposed Methodology for classification of urban LULC. Obtained results and discussions about the observed changes in the classified images are revealed in Sect. 4. At last, conclusion and future works are exhibited in Sect. 5.

2 Study Areas

Aurangabad City (see Fig. 1) is located in the north central part of Maharashtra. This city has many tourist places like Ajanta and Ellora caves, Bibika Maqbara and Deogiri fort, etc. [5].

The atmosphere of the Aurangabad region and its surrounding are identify as a hot summer and dryness atmosphere amid the year except from June to September; whereas post monsoon season start from the month of October to November [6]. The temperatures begin to fall rapidly in November, and December month is considered to be a very coldest and mean min temp is near about 10 °C, and the mean max temp

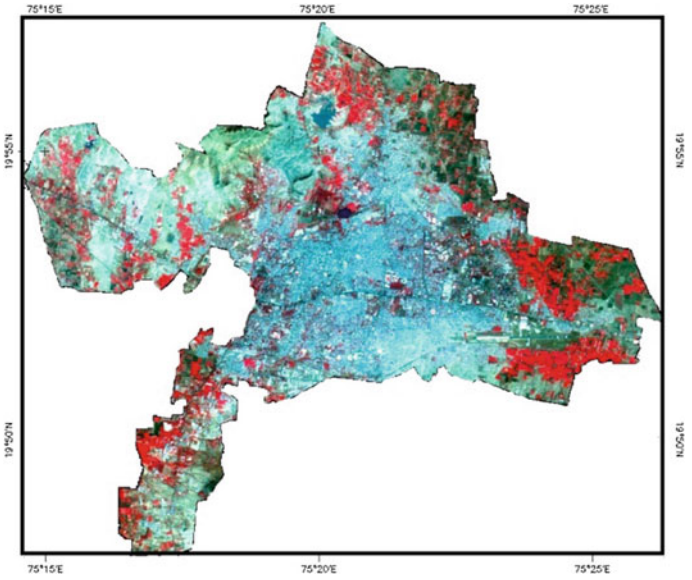

Fig. 1 Area under study

is near about 28 °C. The daily temperature increases from the beginning of March and May and these months are considered to be hottest months with mean minimum temp. of 24 °C and mean max temp. of 40 °C [7]. Therefore December to March is considered to be the best suitable months to identify a LULC of Aurangabad city. According to this, the LISS-III temporal datasets of December-2003, January-2009, and February-2015 have been used for the current study.

3 Proposed Methodology

The literature shows that the multispectral data has been used for the detection of LULC classes. As a result of growing urban improvement and mapping costs city experts keen on viable urban LULC mapping and change detection that can be utilized for improvement in Smart City projects.

The methodology adopted for urban classification of Multispectral images is shown in Fig. 2. As per the study area, the remote sensing LISS-III images were collected from NRSC Hyderabad (India). These multispectral temporal images are captured from same sensor (i.e., LISS-III) with same season and represent same geographical area but it has been captured in different years (i.e., 2003, 2006, and 2015). The preprocessing was performed on this raw LISS-III images and then selection of training data sets, classification and accuracy assessment was done using ENVI tool.

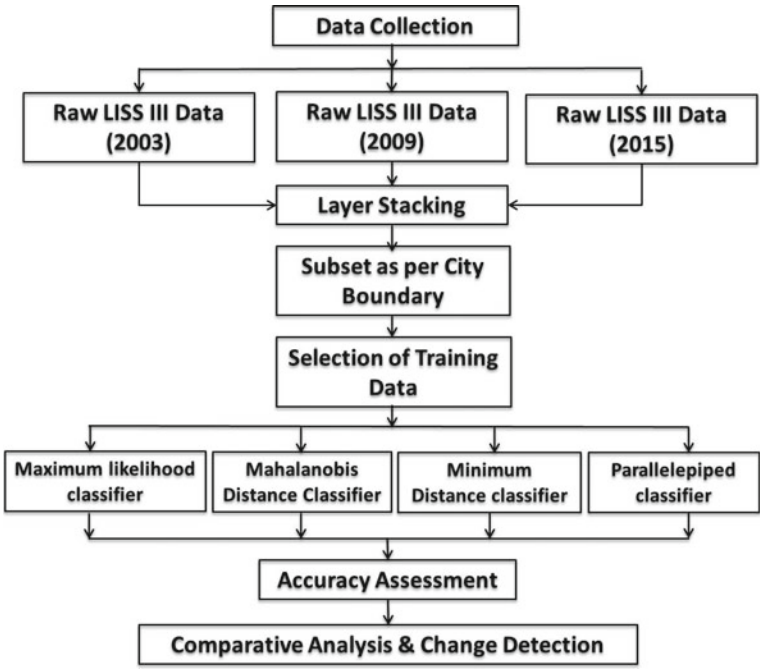

Fig. 2 Proposed methodologies

Table 1 Band specification of LISS-III sensor image

Band	Spectral band (μm)	Spatial resolution (m)
2.	0.52–0.59	23 × 23
3.	0.62–0.68	23 × 23
4.	0.77–0.86	23 × 23
5.	1.55–1.70	23 × 23

3.1 Used Datasets

A Multispectral LISS-3 camera operates in four spectral bands, among these three bands are operates in the Visible-Near-Infrared (VNIR) and 1 operates in the Shortwave-Infrared (SWIR) region [7]. The LISS-III camera provides data with a spatial resolution of 23.5 m. An optical LISS-3 sensor works in four different spectral bands (i.e., Green, Red, NIR, and SWIR). This multispectral sensor covers an area of 141 km wide swath with a moderate spatial resolution of 23 m in all four spectral bands [8]. Table 1 shows a detailed specification of LISS III data [7].

3.2 Preprocessing

Raw LISS III data contains four bands and every band having a separate file. The individual bands for each image are Tagged Image Format File (.TIFF) format. These images are Georeferenced images and having a World Geodetic System (WGS) 1984 Datum (Datum: D_WGS_1984) and projected in UTM Zone 43 N. The raw LISS-III data has four bands which are present in the TIFF format, i.e., Band2 (Green), Band3 (Red), Band4 (NIR), and Band5 (SWIR). The infrared band was utilized in the analysis because its capability detecting vegetation area. Then the Layer Stacking operations were performed and all four bands are comprised in a single image [8].

A single LISS-III image covers near about 24,000 km^2 area of earth surface and Aurangabad Municipal Corporation is our Region of Interest (ROI) and its total area is near about 142 km^2. So, there is need to perform a spatial subset of image and it is achieved by using shape file of Aurangabad corporation area [7]. Spatial Subset (clipping) is a way of reducing the extended area of an image to include just the area that is of interest. In digital image interpretation; most of the times a whole satellite images are not interpreted, only some certain areas of the satellite image were interpreted. In these cases the part we are interested it should be cut (clipped) from the whole image; so it also reduced the size of an image and improve the processing speed and reliability.

3.3 Selection of Training Data

The training pixels have been selected based on their spectral signature for identified LULC classes; with reference to ground truth information which was collected by using GPS-enabled system. The ground truth points were collected during the period of March to April 2015. The collected ground truth points were matched with the 2015 image. The Google earth and visual inspection was used for collection of the old points for 2003 and 2009 images. Moreover, the tested region was well known to us; so the error was less for identifying correct objects and training the data. The six objects were considered for classification namely Residential (Built-up) area, Hill without Vegetation (Rock), Water Body, Vegetation, Fallow Land and Barren Land. The Fig. 3 shows the average spectra of training pixels of selected LULC classes. These selected training pixels were used for classification.

3.4 Classification

A Digital image classification is a mingled process and that requires a different divers factors and it is very challenging task. These factors are selection of RS data, image processing and selection of classification technique. In image classification the prime

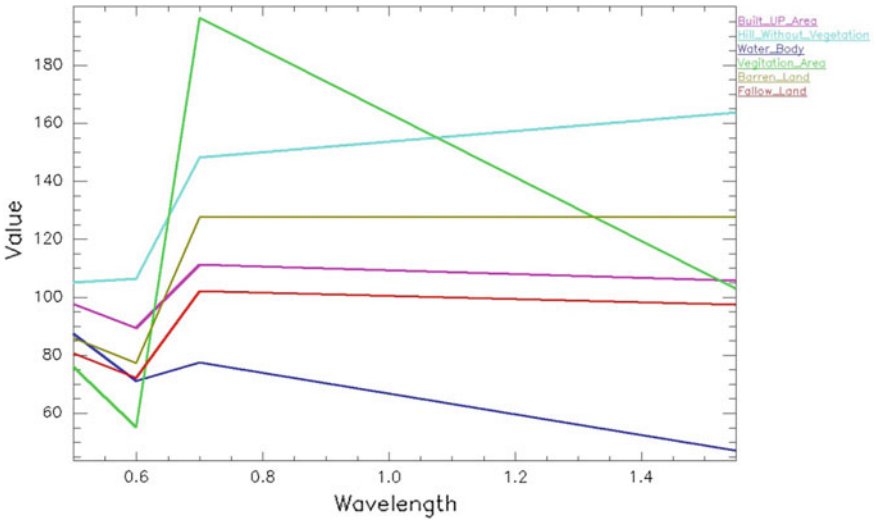

Fig. 3 Average spectra of similar objects used for classification

Table 2 LULC classes along with Anderson LULC code

Sr. No.	Anderson scheme code	Class name	Color
1	1	Residential (built-up) area	Magenta
2	6	Hill without vegetation (Rock)	Cyan
3	5	Water body	Blue
4	2, 4	Vegetation	Green
5	7	Barren land	Yellow
6	3	Fallow land	Red

steps are selection of appropriate classification system, selection of and number of training samples, techniques of image preprocessing, selection of feature extraction technique, post classification processing, and performing accuracy assessment [9]. The motive of classification is to categorize all image pixels into different land-cover classes. This classified data will be used to design thematic maps of the LULC. Table 2 describes the LULC classes for classification of images along with color codes and Anderson LULC code.

3.4.1 Maximum Likelihood Classifier (MLC)

The MLC supervised classification algorithm takes advantages of probability density functions which are used in the classification. It works on overlapping signatures with the help of probability. This classifier is based on Bays theorem, in which an every pixel belongs to the maximum likelihood, are characterized into the related

classes [10]. The probability density functions are estimated by two weighting factors through Bayes theorem [11]. Firstly, the user trains the a priori probability or specific signatures of the class in the given image. Second, for each class the cost of misclassification is weighted as per its probability. Both factors outcomes better decreasing the misclassification [12]. This classifier classifies an unknown pixel's spectral response patterns through assessing both the variance and covariance of the class. The user must have the knowledge about the spectral signature or ground truth [13]. This classifier uses a probability density functions to classify undefined pixel by calculating the probability of every pixel value belonging to each category, after this, the pixel would be assigned to the most likely class with highest probability value. If the probability values are all below a threshold then it labeled as "unknown" [14]. The basic discriminant function for pixel X is,

$$\mathrm{X} \in \mathrm{C_j} \text{ if} \left(\mathrm{C_j/X}\right) = \max\left[\mathrm{p(C_1/X)}, \mathrm{p(C_2/X)}, \ldots, \mathrm{p(C_m/X)}\right], \tag{1}$$

where, the function $\max\left[\mathrm{p(C_1/X)}, \mathrm{p(C_2/X)}, \ldots, \mathrm{p(C_m/X)}\right]$ returns the highest probability. For identification of pixel X it uses the information class resultant to the probability. The Function $p(Ci/X)$ represents a pixel X's conditional probability as being a member of class Cj. The Bayes's theorem is used to solve this problem [10],

$$P\left(C_j/X\right) = p\left(X/C_j\right) * p\left(C_j\right)/p(X) \tag{2}$$

where, Function $p\left(X/C_j\right)$ is a priori probability or conditional probability, and $p\left(C_j\right)$ is the occurrence probability of class Cj in the input data and $p(X)$ is the probability of pixel X occurring in the input data and written as follows [10]:

$$p(X) = \sum_{j=1}^{m} p\left(X/C_j\right) * p\left(C_j\right) \tag{3}$$

where, $p(X)$ is supposed as normalization constant to confirm $\sum_{j=1}^{m} p\left(C_j/X\right)$ equals to 1 and m is the number of classes [10]. While implementation of this classifier, the user gives the opportunity for stating the probability of each information class, therefore the class of a posterior probability can be written as follows

$$p\left(C_j/X\right) = \frac{p\left(X/C_j\right)p\left(C_j\right)}{\sum_{j=1}^{m} p\left(X/C_j\right)p\left(C_j\right)}, \tag{4}$$

where, $p\left(C_j\right)$ is the prior probability of class C_j and $p\left(X/C_j\right)$ is the conditional probability of observing X from class C_j. Therefore the computation of $p(Cj/X)$ is reduced to determination of $p\left(X/C_j\right)$. The analysis of this function can be expressed as for the remote sensing images [10]:

$$p(X/C_j) = \frac{1}{(2\pi)^{n/2}\left|\sum j\right|^{0.5}} \times \exp\left[-\frac{1}{2}(DN - \mu_j)^T \sum_j^{-1}(DN - \mu_j)\right], \quad (5)$$

where; $DN = (DN_1, DN_2, \ldots, DN_n)^T$ is a vector of pixel with n no. of bands; $\mu_j = (\mu_{j1}, \mu_{j2}, \ldots, \mu_{jn})^T$ is a mean vector of the class C_j and $\sum j$ is the covariance matrix of class C_j which can be written as:

$$\sum j = \begin{bmatrix} \sigma_{11} & \sigma_{12} & \ldots & \sigma_{1n} \\ \sigma_{21} & \sigma_{22} & \ldots & \sigma_{2n} \\ \ldots & \ldots & \ldots & \ldots \\ \sigma_{n1} & \sigma_{n2} & \ldots & \sigma_{nm} \end{bmatrix} \quad (6)$$

3.4.2 Mahalanobis Distance (MD)

MD classifier is very similar to Minimum Distance-to Means, except that a covariance matrix is used in this Eq. 7 [14]. Mahalanobis classifier is a Manhattan distance classifier which is dissimilar from Euclidian distance due to its simplicity. For classification and analysis of various patterns it's depend on correlations between variables. Also it measures the similar class of an unknown data set using known data. This classifier uses each band to classify the objects which are the statistical summation of the complete dissimilarities between two pixels in the similar band. The differentiations of pixel values are neglected in deriving the difference [10, 15]. The Eq. (7) for the Mahalanobis distance classifier is as follows:

$$D = (X - M_c)^T (Cov_c^{-1})(X - M_c), \quad (7)$$

where

D	Mahalanobis distance
c	a particular class
X	the measurement vector of the candidate pixel
M_c	the mean vector of the signature of class c
Cov_c	the covariance matrix of the pixels in the signature of class c
cov_c^{-1}	inverse of Cov_c
T	transposition function

The pixel is assigned to the class, c, for which D is the lowest.

3.4.3 Minimum Distance-to Means (MDM)

The MDM is computationally simple which takes the average spectral values within each class signature. It ignores the covariance and standard deviation which are

helpful in classification of different unidentified objects of the image [13]. Hence it uses the unknown image data to classes which minimize the distance between the image data and the class in multi feature space for classification with maximum similarity. For all classes the average spectral value in each band is considered. Therefore, the classifier is mathematically simple and computationally able with some drawbacks [10, 14].

The following equation indicates the decision rule behind this classifier:

$$Pixel\ X \in C_j \text{ if } d(C_j) = \min[d(C_1), d(C_2), \ldots d(C_m)] \tag{8}$$

where;

- $\min[d(C_1), d(C_2), \ldots d(C_m)]$ is a function for identifying the smallest distance among all those inside the bracket
- $d(C_j)$ refers to Euclidean distance between pixel X and the center of information class C_j.

It is calculated using the Eq. (9):

$$d(Cj) = \sqrt{\sum_{i=1}^{n} [DN(i,j) - Cij]^2} \tag{9}$$

The above formula is repeated *m* times with all information classes, for each pixel in the input remote sensing data.

3.4.4 Parallelepiped Classifier

The PC is a box classifier whose opposite sides are straight and equivalent. This classifier uses the class limits and stores it in each class to establish whether a specified pixel falls within the class or not. It is a very simple classifier for computation when speed is necessary with less accuracy and most of the pixels overlap in classification [14].

This classifier assigns pixel into one of the predefined information classes in terms of its value in relation to the DN range of each class in the same band.

$$\text{Pixel X} \in C_i \text{ if Min } DN_i \leq DN_x \leq \text{Max } DN_i \tag{10}$$

where:

Ci Information Class
DN_i DN Value of Information Class
X Pixel
DN_x DN Value of pixel X.

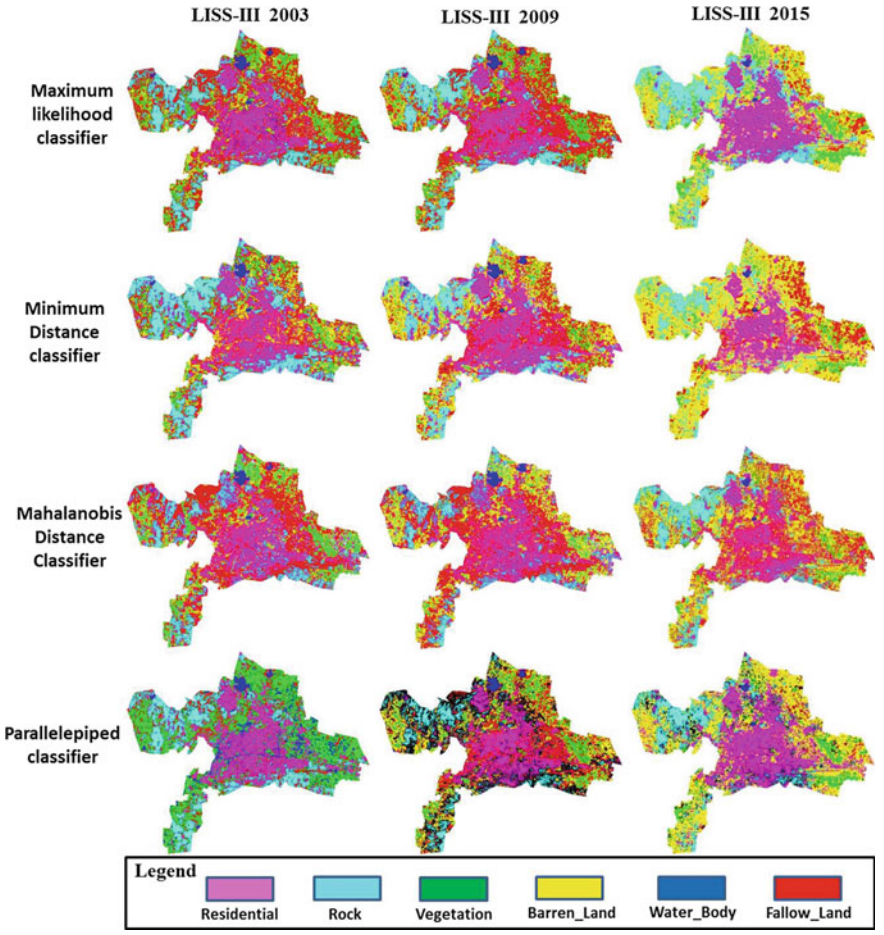

Fig. 4 Classified images of LISS-III multi-temporal data by using four supervised classifiers

The Multitemporal LISS-III datasets of December-2003, January-2009 and February-2015 was classified by using four supervised classifiers. These four classifiers were MLC, MD, MDM and PC and these classifiers are well known and well reported in literature. Figure 4 shows classified images of LISS-III Multitemporal data by using four supervised classifiers.

4 Results and Discussion

The confusion matrix was generated for accuracy assessment of all methods and obtained results are indicated in Tables 3, 4 and 5. The results were evaluated on the basis of overall accuracy, producer's accuracy, user's accuracy and kappa coefficient; computed with reference to confusion matrix. These values are used to compare the results of classification. The said methods have provided the class specific accuracies (Tables 3, 4 and 5). An overall accuracy of the classification is simply defined as the total number of correct classifications divided by the total number of sample points. The producer's accuracy measures how well a certain area has been classified. The producer's accuracy is derived by dividing the number of correct pixels in one class divided by the total number of pixels as derived from reference data. The user's accuracy is therefore a measure of the reliability of the map; it indicates how well the classified map represents what is really on the ground. It is defined as the correct classified pixels in a class are divided by the total number of pixels that were classified in that class [14]. The kappa coefficient measures the agreement between classification and ground truth values. A kappa value of 1 represents perfect agreement; a value of 0 represents no agreement while −1 represents complete disagreement. This is another measure of agreement or accuracy based on the difference between the actual agreement in the error matrix (i.e., the agreement between the remotely sensed classification and the reference data as indicated by the major diagonal) and the chance agreement which is indicated by the row and column total marginal [15].

According to the results of 2015, it is observed that, there were misclassification between barren land and residential area due to its spectral similarity. In fact, all the classes were classified accurately except residential region and barren land using MLC method. However, the MD, MDM, and PC algorithms have given the similar error for residential area, barren land and fallow land due to because of their spectral resemblance. Additionally, the misclassification was found to be normal with vegetation and hill without vegetation using all methods. On the other hand, the results of 2015, 2009, and 2003 were similar for water bodies and vegetation areas. The other classes were also classified well except barren land with 2015, 2009, and 2003 images using all methods. Furthermore, whatever the misclassification were identified, it was due to similarity in reflectance behavior of said LULC classes.

The results clearly indicates that, the MLC has given the highest overall accuracy of 73.07%, 83.51%, and 93.43% with kappa coefficient of 0.64, 0.78, and 0.90 in 2003, 2009 and 2015 respectively. The MLC is a standout among the most mainstream techniques for characterization in remote sensing as compared to other supervised classifiers. The obtained results were compared with others as given in Table 6, and it is found to be better. As per accuracy assessment a MLC was considered for comparing the LULC change detection.

Table 3 Accuracy assessment of LISS-III 2015 classified images

Class name	Maximum likelihood			Mahalanobis distance			Minimum distance			Parallelepiped classifier		
	PA	UA	OA/ƙ	PA	UA	OA/ƙ	PA	UA	OA/ƙ	PA	UA	OA/ƙ
RA	97.44	100	**93.43/0.90**	79.49	68.89	**83.01/0.76**	89.74	100	**88.41/0.84**	79.49	100	**81.46/0.75**
HWV	100	86.72		97.3	87.8		94.59	88.24		98.2	87.2	
WB	100	100		100	100		100	81.82		100	100	
VA	100	100		76.92	100		96.15	100		76.92	100	
BL	5.88	100		23.53	33.33		23.53	28.57		5.88	14.29	
FL	100	100		64.1	78.13		84.62	100		58.97	100	

OA overall accuracy, *PA* producer's accuracy, *UA* user's accuracy, *ƙ* Kappa coefficient, *RA* residential area, *HWV* Hill without vegetation, *WB* water body, *VA* vegetation area, *BL* Barren Land, *FL* Fallow land

Table 4 Accuracy assessment of LISS-III 2009 classified images

Class name	Maximum likelihood			Mahalanobis distance			Minimum distance			Parallelepiped classifier		
	PA	UA	OA/ƙ	PA	UA	OA/ƙ	PA	UA	OA/ƙ	PA	UA	OA/ƙ
RA	94.74	100	**83.51/0.78**	57.89	40.74	**70.87/0.61**	100	61.29	**82.41/0.76**	84.21	100	**79.12/0.73**
HWV	100	44.74		88.24	48.39		100	50.00		94.12	84.00	
WB	100	100		100	100		100	100		97.37	100	
VA	100	100		93.33	100		100	100		93.33	100	
BL	25.00	38.00		12.00	25.00		3.23	100		0.00	0.00	
FL	100	68.57		54.17	39.39		100	96.00		100	88.89	

Table 5 Accuracy assessment of LISS-III 2003 classified images

Class name	Maximum likelihood			Mahalanobis distance			Minimum distance			Parallelepiped classifier		
	PA	UA	OA/ƙ	PA	UA	OA/ƙ	PA	UA	OA/ƙ	PA	UA	OA/ƙ
RA	89.47	100	**73.07/0.64**	78.95	46.00	**66.85/0.57**	94.74	54.55	**64.84/0.54**	94.74	69.23	**68.13/0.58**
HWV	94.12	59.26		76.47	59.09		100	45.95		94.12	53.33	
WB	94.74	100		92.00	100		84.21	100		94.74	84.71	
VA	86.67	92.86		80.00	100		86.67	100		93.33	63.64	
BL	21.26	30.00		16.45	26.30		5.43	16.79		0.00	0.00	
FL	62.50	35.71		50.00	31.58		25.00	54.55		16.67	22.22	

Table 6 Results comparison with others published work

Author and year	Purpose	Data used	Techniques	Accuracy (%)
Kamrul Islam (2017) [1]	LULC CD	Landsat 5 TM, Landsat 8 OLI/TIRS	MLC	83.96–92.16
Sinha et al. (2015) [16]	Improved LULC classification	Landsat ETM+	MLC	85
Jayanth et al. (2016) [17]	LULC change detection (CD)	LISS-IV, CARTOSAT-1	Support vector machine artificial bee colony (ABC), MLC	62.63–80.4
Butt et al. (2015) [18]	LULC CD	Landsat TM, SPOT-5	MLC, post classification refinement	90
Beuchle et al. (2015) [19]	LULC CD	Landsat TM, Landsat ETM	Object-based classification	85–90
Our proposed work	LULC CD	LISS-III	MLC, MD, MDM and PC	73.07–93.43

4.1 Change Detection

The purpose of present study is not only to classify the LULC, but also to identify the temporal changes in the region. Effective application of geospatial technology for LULC change discovery to a great extent depends on an appropriate understanding of the study area. Change detection of LISS-III temporal datasets of December-2003, January-2009 and February-2015 shown in Table 7; it shows all results in percentage which was computed by considering the number of classified pixels of each class and total number of classified pixels. As per the results, there is a growth in residential area of 1.24% in 2009 and 11.34% in 2015 as compared to 2003. Since from 2003 the rainfall was remarkably decreased every year in Aurangabad region till 2015, this makes effects on the storage of water bodies in the region and it is clearly observed that, water body area has been decreased by 1.23% in 2009 and 1.9% in 2015 as compared to 2003. This less rainfall make effects on the vegetation area and it has been decreased by 1.96% and 3.69% in 2009 and 2015 respectively. The vegetation's were available with rock surface regions in 2003; however it (vegetation) was reduced in 2009 and 2015. Consequently the rocks were highlighted more in 2009 and 2015 by 1.72% and 3.27% respectively as compared to 2003. Due to fast urban expansion, the fallow Land was decreased by 1.09% and 33.98% in 2009 and 2015 respectively; which is converted into Barren Land, hence barren land is increased by 1.29% and 24.94% in 2009 and 2015 as compared to 2003. Figure 5 shows the Statistical analysis of LISS III Temporal Datasets obtained from MLC.

Table 7 Change detection of LISS-III 2003, 2009 and 2015 by using MLC

Sr. no.	Class name	Color	LISS-III classification			Remark
			2003 (%)	2009 (%)	2015 (%)	
1	Residential	Magenta	17.16	18.40	28.50	Increased
2	Rock	Cyan	18.35	20.07	21.62	Increased
3	Water_Body	Blue	2.20	0.97	0.30	Decreased
4	Vegetation	Green	12.58	10.62	8.89	Decreased
5	Barren_Land	Yellow	10.21	11.50	35.15	Increased
6	Fallow_Land	Red	39.52	38.43	5.54	Decreased

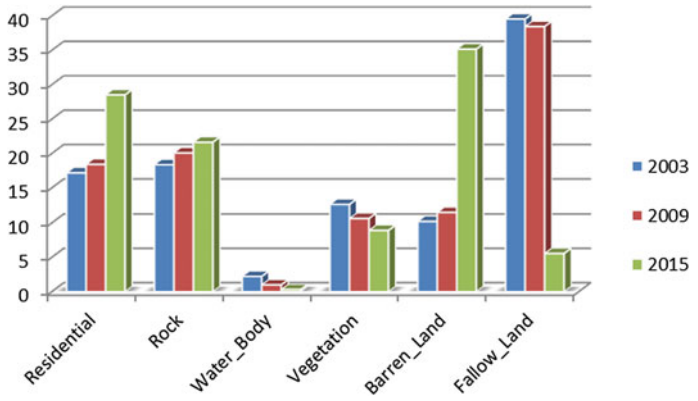

Fig. 5 Statistical analysis of LISS III temporal datasets obtained from MLC

5 Conclusions

LULC is important factor in comprehensible the relations between the human activities and the environment. Satellite Remote sensing systems have an ability to cover a large area. This research reports a Mapping of LULC classification using LISS-III multispectral image datasets of December 2003, January 2009, and February 2015 of the Aurangabad Municipal Corporation (AMC) area. As IIRS LISS-III data sets used in this study having 23.5 m spatial resolution and four spectral bands, this spatial and spectral characteristic gives enough details for LULC mapping and change detection. The LULC classes are derived from a level one classification of the Anderson classification schemes. In the study, MLC has given highest accuracy as compared to other supervised classifiers; hence MLC is the most recommended technique to perform classification and mapping. To achieve the better accuracy with maximum LULC classes (Anderson Level 2), very high spatial resolution Multispectral data can be used.

Acknowledgements Author(s) would like to acknowledge, UGC-BSR Fellowships, DST_FIST and UGC-SAP(II) DRS Phase-I and Phase-II F.No.-3-42/2009 & 4-15/2015/D R S -II for Laboratory Facility to Department of CS & IT, Dr. B.A.M.University, Aurangabad (MS), INDIA.

References

1. Islam, K., Jashimuddin, M., Nath, B., Nath, T.K.: Land use classification and change detection by using multi-temporal remotely sensed imagery: the case of Chunati wildlife sanctuary, Bangladesh. Egypt. J. Remote Sens. Space Sci. (2017)
2. Rawat, J.S., Kumar, M.: Monitoring land use/cover change using remote sensing and GIS techniques: a case study of Hawalbagh block, district Almora, Uttarakhand, India. Egypt. J. Remote Sens. Space Sci. **18**(1), 77–84 (2015)
3. Reis, S.: Analyzing land use/land cover changes using remote sensing and GIS in Rize, North-East Turkey. Sensors **8**(10), 6188–6202 (2008)
4. Lu, D., Mausel, P., Brondízio, E., Moran, E.: Change detection techniques. Int. J. Remote Sens. **25**(12), 2365–2401 (2004). https://doi.org/10.1080/0143116031000139863
5. Nagne, A.D., Dhumal, R.K., Vibhute, A.D., Rajendra, Y.D., Kale, K.V., Mehrotra, S.C.: Suitable sites identification for solid waste dumping using RS and GIS approach: a case study of Aurangabad, MS, India. In: 2014 Annual IEEE India Conference (INDICON), pp. 1–6. IEEE (2014)
6. Balpande, U.S.: Ground_Water Information of Aurangabad District Maharashtra, Ministry of Water Resources Central Ground Water Board, Gov. of India, 1791/DBR/201. http://cgwb.gov.in/District_Profile/Maharashtra/Aurangabad.pdf
7. Nagne, A.D., Dhumal, R.K., Vibhute, A.D., Gaikwad, S., Kale, K., Mehrotra, S.: Land use land cover change detection by different supervised classifiers on LISS-III temporal datasets. In: 2017 1st International Conference on Intelligent Systems and Information Management (ICISIM) (2017)
8. Resourcesat—1 Data User's Handbook, National Remote Sensing Agency, Department Of Space, Govt. Of India NrsaBalanagar, Hyderabad—500037, A.P. India. http://Bhuvan.Nrsc.Gov.In/Bhuvan/Pdf/Resourcesat-1_Handbook.Pdf
9. Hebbara, R., SeshaSaib, M.V.R.: Comparison of LISS-IV MX AND LISS-III+ LISS-IV merged data for classification of crops. ISPRS Ann. Photogramm. Remote Sens. Spatial Inf. Sci. (ISPRS Technical Commission VIII Symposium, 09–12 December 2014, Hyderabad, India) **II**(8) (2014)
10. Vibhute, A.D., Dhumal, R.K., Nagne, A.D., Rajendra, Y.D., Kale, K.V., Mehrotra, S.C.: Analysis, classification, and estimation of pattern for land of Aurangabad region using high-resolution satellite image. In: Proceedings of the Second International Conference on Computer and Communication Technologies, pp. 413–427. Springer, New Delhi (2016)
11. Govender, M., Chetty, K., Bulcock, H.: A review of hyperspectral remote sensing and its application in vegetation and water resource studies. Water SA **33**(2) (2007). ISSN 0378-4738. Water SA (on-line). ISSN 1816-7950. http://www.wrc.org.za
12. Srivastava, P.K., Han, D., Rico-Ramirez, M.A., Bray, M., Islam, T.: Selection of classification techniques for land use/land cover change investigation. Adv. Space Res. **50**(9), 1250–1265 (2012)
13. Murtaza, K.O., Romshoo, S.A.: Determining the suitability and accuracy of various statistical algorithms for satellite data classification. Int. J. Geomat. Geosci. **4**(4), 585 (2014)
14. Gao, J.: Digital Analysis of Remotely Sensed Imagery. McGraw-Hill Professional (2008)
15. Banko, G.: A review of assessing the accuracy of classifications of remotely sensed data and of methods including remote sensing data in forest inventory (1998)
16. Sinha, S., Sharma, L.K., Nathawat, M.S.: Improved land-use/land-cover classification of semi-arid deciduous forest landscape using thermal remote sensing. Egypt. J. Remote Sens. Space Sci. **18**(2), 217–233 (2015)

17. Jayanth, J., Kumar, T.A., Koliwad, S., Krishnashastry, S.: Identification of land cover changes in the coastal area of Dakshina Kannada district, South India during the year 2004–2008. Egypt. J. Remote Sens. Space Sci. **19**(1), 73–93 (2016)
18. Butt, A., Shabbir, R., Ahmad, S.S., Aziz, N.: Land use change mapping and analysis using Remote Sensing and GIS: a case study of Simly watershed, Islamabad, Pakistan. Egypt. J. Remote Sens. Space Sci. **18**(2), 251–259 (2015)
19. Beuchle, R., Grecchi, R.C., Shimabukuro, Y.E., Seliger, R., Eva, H.D., Sano, E., Achard, F.: Land cover changes in the Brazilian Cerrado and Caatinga biomes from 1990 to 2010 based on a systematic remote sensing sampling approach. Appl. Geogr. **58**, 116–127 (2015)